Available online at www.sciencedirect.com
ScienceDirect
Advances in Space Research 38 (2006) 1509–1519
ADVANCES IN SPACE RESEARCH (a COSPAR publication)
www.elsevier.com/locate/asr

XMM-*Newton* spectroscopy of stars in open clusters and star forming regions

R. Pallavicini *, E. Franciosini, A. Maggio, L. Scelsi [1], J. Sanz-Forcada [2]

INAF-Osservatorio Astronomico di Palermo, Piazza del Parlamento 1, I-90134 Palermo, Italy

Received 22 October 2004; received in revised form 24 March 2005; accepted 31 March 2005

Abstract

We discuss observations of open clusters and star forming regions obtained with the RGS and EPIC instruments on board XMM-*Newton*. These observations provide a powerful tool to investigate the temperature structure, emission measure distribution and elemental abundances of stars from the pre-main sequence phase to post-main sequence evolution. We report in particular on EPIC and RGS spectroscopy of hot and cool stars in the very young cluster around σ Orionis, of two stars in the Hyades (the main-sequence star VB 50 and the clump giant VB 71) and of two pre-main sequence stars in Taurus–Auriga (the classical T Tauri star SU Aur and the weak-lined T Tauri star HD 283572). The implications of these observations for models of magnetic activity in late-type stars, of wind emission in early-type stars, and of X-ray production in the early stages of stellar evolution are briefly discussed.

Keywords: Stars: late-type; Stars: early-type; Stars: pre-main sequence; X-rays: spectroscopy; Open clusters; Star forming regions

1. Introduction

Open clusters (OCs) constitute homogeneous samples of stars with approximately the same age, distance and chemical composition. Because of this, they are fundamental tools to study stellar structure and evolution as well as the dependence of chromospheric and coronal activity on stellar rotation and dynamo-generated magnetic fields. The observations show that the X-ray emission of late-type stars in clusters is a strong function of magnetic activity as measured, e.g., by the Rossby number (a combination of rotation and convective zone properties believed to measure the efficiency of the dynamo process). Since late-type convective stars suffer magnetic braking during their evolution on the main sequence (MS), the level of coronal X-ray emission is expected to be a declining function of age through the influence of stellar rotation on the efficiency of the dynamo process. Early observations by *Einstein* and ROSAT have by and large confirmed these expectations, but they have also shown that the relationship between activity, age and rotation is much more complex than hitherto suspected (Jeffries, 1999; Randich, 2000 and references therein).

X-rays have proven to be a key diagnostic tool also for the study of star forming regions (SFRs) and of the early evolution of pre-main sequence (PMS) stars. They allow us to peer deep, as much as infrared observations, in the highly absorbing cores of molecular clouds, and to study the relative role of X-ray production mechanisms (e.g., accretion vs. coronal activity) in young stellar objects (YSOs). We remind the reader that star formation is a rapid but quite complex process, that leads, in just a few million years, from an infalling

* Corresponding author.
E-mail addresses: pallavic@astropa.unipa.it, pallavic@oapa.astropa.unipa.it (R. Pallavicini).
[1] Present address: DISFA, Università di Palermo, Italy.
[2] Present address: Astrophysics Division, ESTEC, Noordwijk, The Netherlands.

0273-1177/$30
doi:10.1016/j.asr.2005.03.147

protostar to a diskless zero-age MS star, through various successive stages. It is generally believed (e.g., Feigelson and Montmerle, 1999) that the early-evolution of low-mass YSOs passes successively through the stages of infalling protostar (Class 0, age $\sim 10^4$ yr), evolved protostar (Class I, $\sim 10^5$ yr), Classical T Tauri star (CTT or Class II, $\sim 10^6$–10^7 yr), weak-lined T Tauri star (WTT or Class III, $\sim 10^6$–10^7 yr) and finally to that of zero-age main-sequence (ZAMS) star (age $>10^7$ yr). Except for Class 0 objects, for which the existence of X-ray emission is still a matter of debate, X-rays have been detected from all other classes, and in particular in Class II and III objects, at levels orders of magnitude larger than in the Sun and other inactive solar-type stars. Particularly relevant in this context is the comparison of CTT and WTT stars, which have both strong X-ray emission and similar ages, but which differ dramatically with regard to the presence or not of a thick circumstellar disk. The crucial issue here is to understand which of two possible processes (i.e., accretion or solar-like magnetic activity) is more important to produce X-ray emission in CTT stars.

Hot stars (spectral types O and B) are also usually present in young OCs and SFRs. These stars lack the convective envelopes that characterize cool stars (spectral types F to M) and hence cannot sustain magnetic field generation by dynamo action; yet they are vigorous X-ray emitters, with X-ray luminosities proportional to bolometric luminosities. Current models indicate that X-ray emission is due in this case to radiative instabilities in their massive winds that lead to the formation of density inhomogeneities and to shock heating throughout the wind. The transition between hot stars with shocked X-ray emitting winds and late-type stars with dynamo-powered coronal emission occurs around spectral type A. Stars of this type should be X-ray dark since they do not possess strong winds nor coronae. Observations confirm this general behavior although several X-ray emitting A-type stars (likely binaries with unseen late-type companions) have been reported in the literature.

As part of the Mission Scientist Guaranteed Time on XMM-*Newton* we have observed several OCs and SFRs spanning the age interval from a few Myr to the age of the Hyades ($\sim$600 Myr). In this paper, we present an overview of this program focussing on spectroscopic results obtained with the Reflection Grating Spectrometer (RGS) at high resolution and with the European Photon Imaging Camera (EPIC) at medium resolution. For an overview of the imaging results of the same program, we refer to Franciosini et al. (2003) and Pallavicini et al. (2004). We report in particular on observations of hot and cool stars in the very young cluster around σ Orionis, of two stars in the Hyades (the MS star VB 50 and the clump giant VB 71), and of two PMS stars in Taurus–Auriga (the CTT star SU Aur and the WTT star HD 283572).

2. Hot and cool stars in the σ Orionis cluster

The σ Ori cluster, discovered by ROSAT around the O9.5V star σ Ori AB, belongs to the OB1b association and is located at a distance of $\sim$350 pc; it contains more than 100 likely PMS stars within 30′ of σ Ori AB (Walter et al., 1997; Sherry et al., 2004). Optical and IR photometric and spectroscopic surveys have detected several very low-mass cluster candidates, including brown dwarfs and planetary-mass objects (Béjar et al., 1999, 2004; Zapatero-Osorio et al., 2000; Scholz and Eislöffel, 2004; Kenyon et al., 2005). The estimated age of the cluster is $\sim$2–5 Myr.

The combined MOS + PN EPIC observation of the σ Ori cluster has an equivalent MOS exposure time of $\sim$200 ks. The sensitivity at the center of the field is $L_X = 2.3 \times 10^{28}$ erg s^{-1} (3σ upper limit). We detected 174 X-ray sources at a significance level $>5\sigma$; 87 were identified with at least one possible cluster counterpart within 5″ of the X-ray position. Of the detected members, four are early-type stars (including the hot stars σ Ori AB and σ Ori E) and seven are very low-mass stars of spectral type later than $\sim$M5, including the brown-dwarf candidate S Ori 25 and the planetary-mass object S Ori 68. However, two of the latter sources (including the one identified with S Ori 68) have another possible counterpart within 5″, and their identification is ambiguous. The latest member with a certain X-ray detection is the brown-dwarf candidate S Ori 25, which has a spectral type M7.5 and an estimated mass of $0.05 - 0.13 M_\odot$; its X-ray luminosity is 3×10^{28} erg s^{-1} (see Franciosini et al., in press for details).

Our pointing at the σ Ori cluster was centered on the hot star σ Ori AB in order to obtain a high-resolution RGS spectrum of this source (Sanz-Forcada et al., 2004). The RGS spectrum is contaminated by the nearby source σ Ori E (another hot star of spectral type B2Vp), whose contribution needs to be subtracted in order to get a clean spectrum of the central source. Two other nearby sources (both late-type stars) could potentially contaminate the RGS spectrum of σ Ori AB, but they are sufficiently far away from the central source to be excluded by the RGS extraction procedure. Fig. 1 shows the light curves of these four sources at the center of the field. Clearly σ Ori AB is the brightest source and its emission is constant (with a 1σ upper limit of 1% to any possible variability). Most interestingly, the other hot star σ Ori E shows instead a strong X-ray flare which is difficult to understand in a hot star (see below). Of the other two sources, Source #3 (a K0 star) is constant, while Source #4 (another K-type star) shows evidence of rotational modulation with a period of $\sim$9 h (Pallavicini et al., 2004). The observed modulation, with an amplitude of $\sim$25%, can be attributed to the inhomogeneous distribution of active regions over the surface of the star.

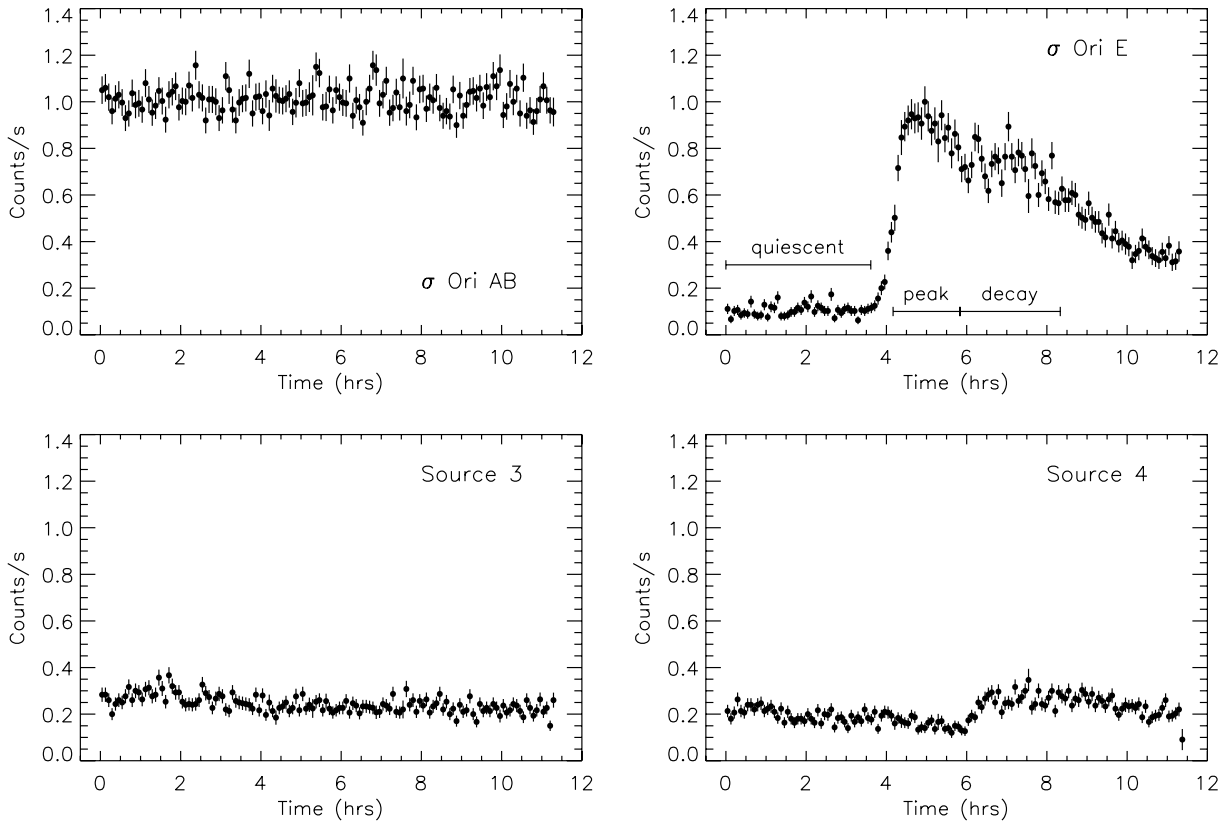

Fig. 1. EPIC PN light curves for the brightest central sources in the σ Ori cluster.

Fig. 2 shows the EPIC spectra of the same sources. σ Ori AB has clearly a much softer spectrum than the other sources. A 2-T thermal fit (assuming the APEC code and fixing $N_H = 2.7 \times 10^{20}$ cm^{-2}) gives $T_1 =$ 0.1 keV, $T_2 = 0.3$ keV, $EM_1 = 2 \times 10^{54}$ cm^{-3}, $EM_2/EM_1 \sim 2$ and Fe $\sim$0.4 Fe$_\odot$. The low X-ray temperature is consistent with X-rays originating in a shocked wind, rather than being due to magnetically confined coronal structures (see discussion in Sanz-Forcada et al., 2004).

The spectrum of σ Ori E shown in Fig. 2 is integrated over the entire observation, and thus includes both the flare emission and the preflare quiescent emission. The statistic is high enough, however, to allow separate spectral fits for both the flare and the preflare quiescent emission. A 2-T spectral fit gives $T_1 = 0.3$ keV, $T_2 = 1.1$ keV, $EM_1 = 7.1 \times 10^{53}$ cm^{-3}, $EM_2/EM_1 = 0.9$ for the quiescent phase, and $T_1 = 0.8$ keV, $T_2 = 3.5$ keV, $EM_1 = 3.6 \times 10^{53}$ cm^{-3}, $EM_2/EM_1 = 9.6$ at the peak of the flare. The quiescent emission is hotter than typically observed in early-type stars and, in particular, it is hotter than in the hot star σ Ori AB. An X-ray flare, detected from the same source by ROSAT, was reported by Groote and Schmitt (2004) who attributed it to the hot star. However, because of the unusually (for a hot star) high temperature of the quiescent preflare corona determined by us with EPIC, we believe it more likely that the flare we observed, and at least part of the quiescent emission, originated from an unseen late-type companion.

Fig. 3 shows the RGS spectra of σ Ori AB. We have analyzed these spectra by correcting for the contribution of σ Ori E and by measuring individual line fluxes to reconstruct the emission measure distribution $EM(T)$ and derive individual elemental abundances (Sanz-Forcada et al., 2004). The results show that: (i) the $EM(T)$ peaks at $\log T \sim 6.7$, consistent with the EPIC results; (ii) there is no evidence of line shifts or broadenings larger than $\sim$800 km s^{-1} as could be produced by *strong* winds; (iii) the weakness of the forbidden lines compared to the intercombination lines in He-like O and Ne could be due either to very high density or, more likely, to the high UV radiation field of the hot star (which allows us to put only uninteresting lower limits on density, but some useful constraints on the location of the X-ray emitting region, cf. Sanz-Forcada et al., 2004). The C, N and O abundances with respect to Fe are higher than solar, but there is no evidence of enhanced N/C ratio. This excludes the presence in the photosphere of the star of dredged-up CNO-cycle processed material, consistently with the star MS evolutionary state.

In addition to the sources discussed above, there are a number of other X-ray sources in the σ Ori field, identified with low-mass PMS stars, that have >1000 cts in the EPIC PN. Spectral fits to these sources give typical

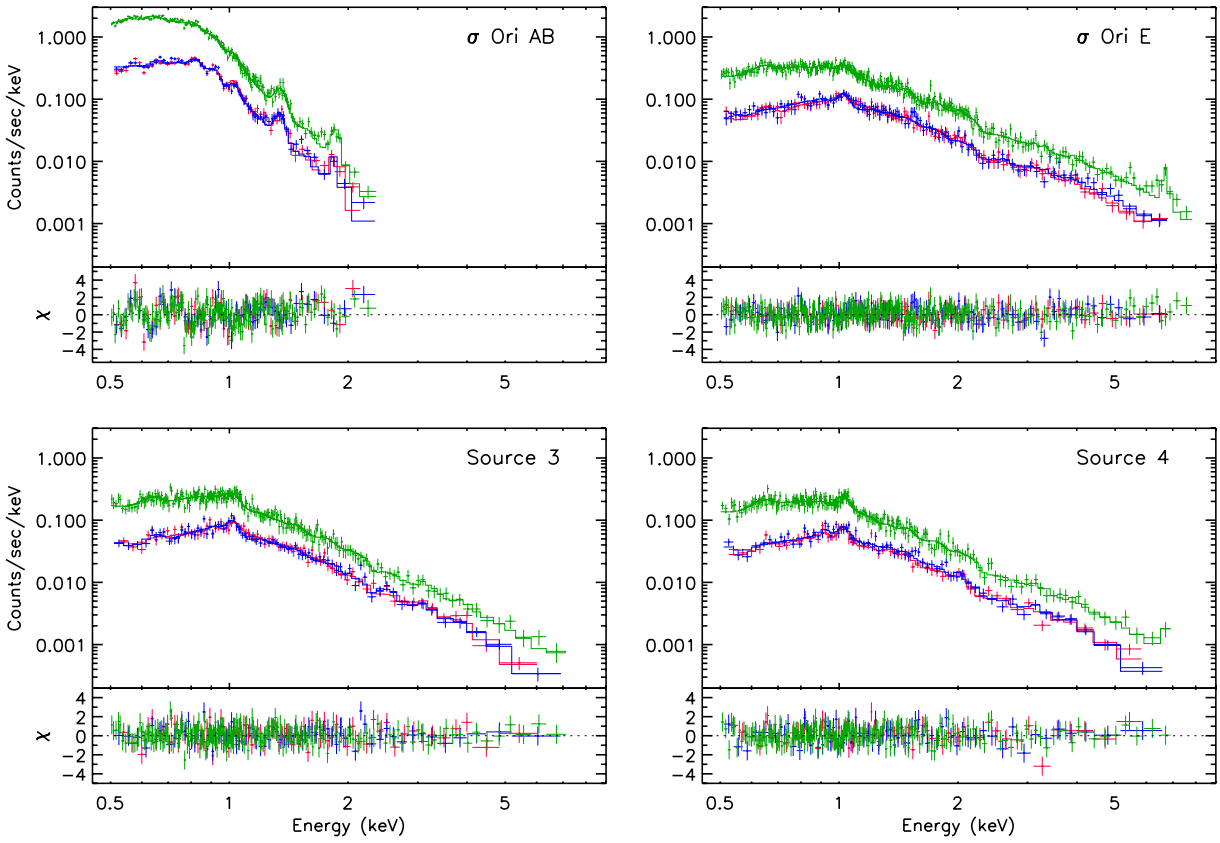

Fig. 2. EPIC MOS and PN spectra and their best fits for the sources shown in the previous figure. Residuals are also shown.

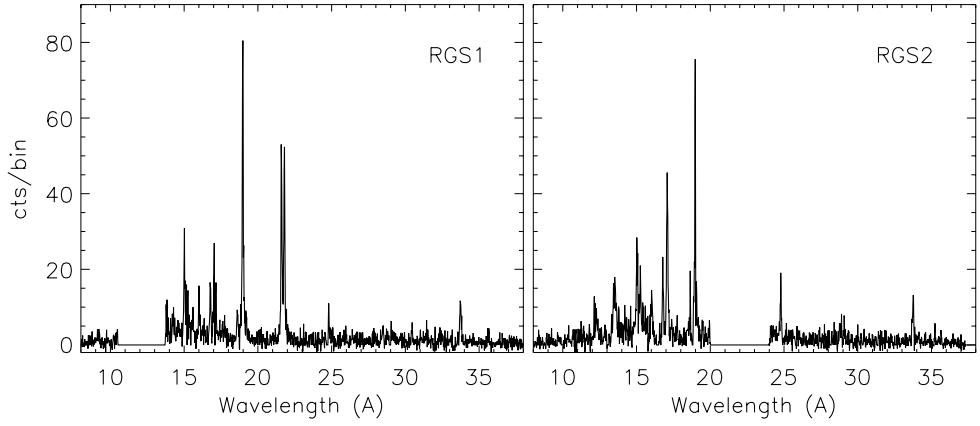

Fig. 3. RGS1 (left) and RGS2 (right) spectra of σ Ori AB. These spectra are contaminated by the nearby source σ Ori E.

values of $T_1 = 0.3$–0.8 keV, $T_2 = 1$–3 keV, $Z = 0.1$–0.3 solar. A comparison of the few WTT and CTT stars in the region with >1000 cts in the PN detector shows no significant differences in the metallicity and temperature of the two classes (Franciosini et al., in press) contrary to what reported by Favata et al. (2003) for the metallicity of PMS stars in L1551. The sample, however, is too small to allow us to draw general conclusions about the existence (or lack) of systematic differences in the spectral properties of CTT and WTT stars (cf. Section 4 below and Stassun et al. (2004) for the Orion Nebula cluster).

3. The Hyades cluster: VB 50 and VB 71

The Hyades (age ~600 Myr) is one of the closest and best studied open clusters. It has been extensively studied in X-rays with *Einstein* and ROSAT and its X-ray luminosity function for late-type stars is well determined

(Stern et al., 1995). The higher sensitivity and spectral resolution of XMM-*Newton* provide an opportunity to determine also the spectral properties of the Hyades stars (temperature structure, emission measure distribution, elemental abundances). However, since the Hyades cluster extends over several square degrees, many different exposures are required to cover a significant fraction of the cluster with XMM-*Newton* (and, a fortiori, with *Chandra*).

We have obtained two observations of the Hyades cluster centered, respectively, on the K-type clump giant VB 71 = θ^1 Tau and on the G-type dwarf VB 50. The two central sources are bright enough for high-resolution RGS spectra. A preliminary source detection on the EPIC fields yielded ~135 sources in the VB 71 field and ~100 sources in the VB 50 field but only a few detected sources in each image are Hyades members. We concentrate therefore on the central sources of the two fields.

Fig. 4 shows EPIC spectra of VB 71 and VB 50. A 2–T fit to the spectra of the clump giant (performed using the APEC model) gives T_1 ~0.3 keV, EM_1 $\sim 4 \times 10^{52}$ cm^{-3}, T_2 ~0.6 keV, EM_2 $\sim 2.5 \times 10^{52}$ cm^{-3}, Fe ~0.9 solar and X-ray luminosity (in the 0.3–8 keV band) $L_X \sim 1.0 \times 10^{30}$ erg s^{-1}; for the G dwarf we obtained instead T_1 ~0.4 keV, EM_1 $\sim 3 \times 10^{52}$ cm^{-3}, T_2 ~1.8 keV, EM_2 $\sim 1 \times 10^{52}$ cm^{-3}, Fe ~0.4 solar and X-ray luminosity $L_X \sim 5.3 \times 10^{29}$ erg s^{-1}. Note the subsolar metallicity of both stars (particularly of the dwarf), which is at variance with the suprasolar photospheric metallicity of the Hyades; note also the higher T_2 temperature and the factor of 2 lower X-ray luminosity of the VB 50 dwarf with respect to the clump giant. However, models that fit the data with a number of discrete isothermal components are only a crude description of the temperature structure of stellar coronae, not to mention the fact that the best fit parameters deduced from the PN and MOS detectors show often significant discrepancies due to as yet unsolved cross-calibration problems (see, e.g., Maggio, 2004). A more physical description of the temperature structure and a more accurate determination of individual elemental abundances can be obtained from the higher resolution RGS spectra. Fig. 5 shows the RGS spectra obtained for the two stars. Lines fluxes can be measured for individual spectral lines of different stages of ionization of

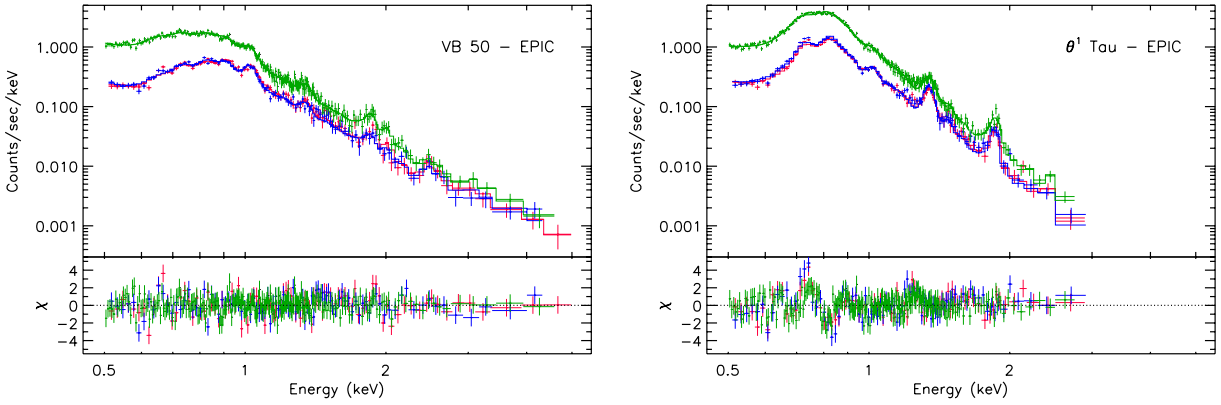

Fig. 4. EPIC spectra of the Hyades stars VB 50 and VB 71 (θ^1 Tau).

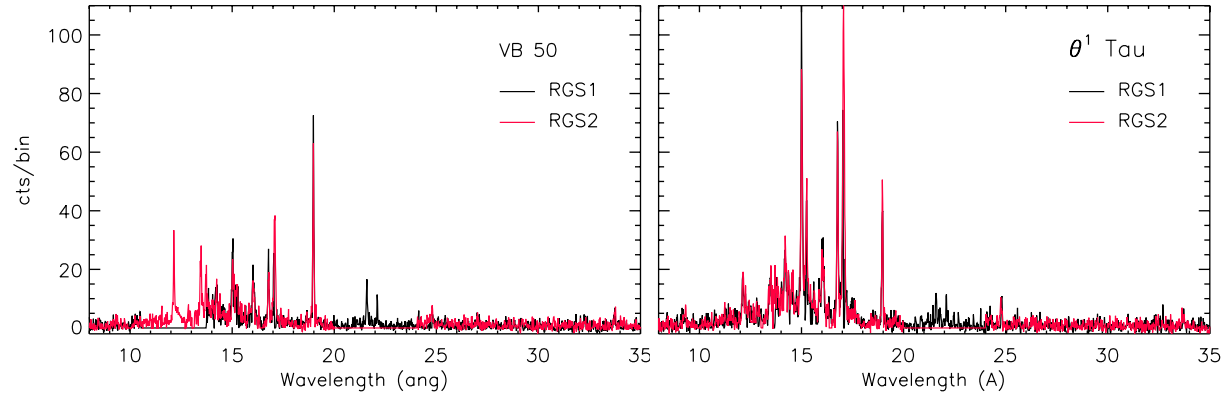

Fig. 5. RGS spectra of the Hyades stars VB 50 and VB 71 (θ^1 Tau).

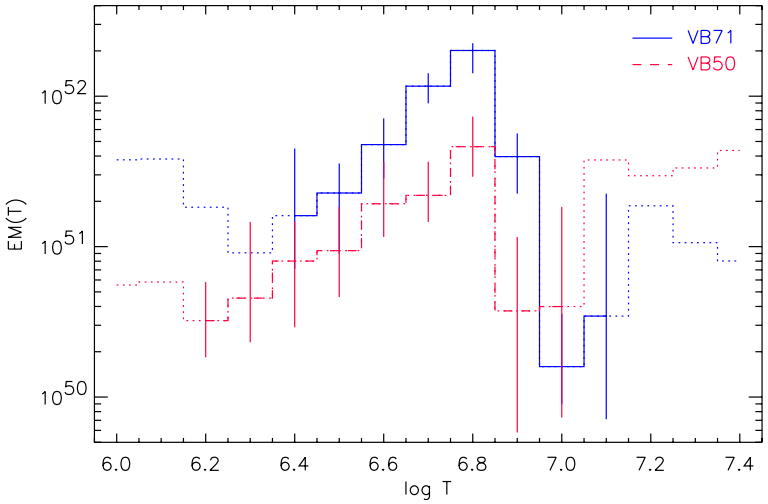

Fig. 6. Emission measure vs. temperature distribution of the Hyades stars VB 50 and VB 71 as derived from line analysis of RGS spectra.

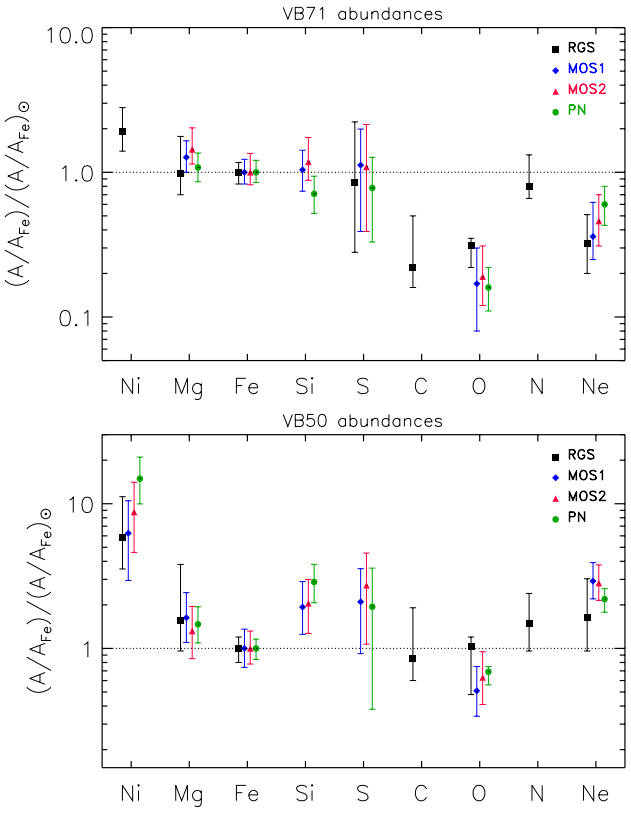

Fig. 7. Element to Fe ratios, relative to solar photospheric values, for VB 71 (upper panel) and VB 50 (lower panel) in the Hyades. Error bars are $\pm 1\sigma$.

the most abundant elements, thus allowing an accurate determination of the chemical composition and of the distribution of the emitting material vs. temperature.

Fig. 6 shows the emission measure distribution as a function of temperature derived for the two Hyades stars using the MCMC method of Kashyap and Drake (1998): both stars peak at $\log T = 6.8$ and show a power-law increase to the maximum $\sim T^{\alpha}$ with $\alpha = 3.0 \pm 0.7$ for VB 71 and 1.9 ± 0.5 for VB 50. These slopes are somewhat lower than the $\sim T^{5}$ slopes found for very active stars (see next section and Scelsi et al., 2004). Fig. 7 shows element to Fe abundance ratios, relative to solar photospheric values, for the most abundant species for both stars. The various elements are ordered with increasing first ionization potential (FIP). While in VB 71 the low-FIP elements behave like solar photospheric abundances, the high-FIP elements (C, O) are strongly underabundant with respect to the Sun, and N is overabundant with respect to C and O, which is evidence for the presence in the corona of the star of dredged-up CNO-cycle material (e.g., Ness, 2005; Audard et al., 2004, see also Lambert and Ries (1981) for similar evidence at photospheric level). This is consistent with VB 71 being a post-He flash clump giant. VB 50 shows solar-like abundance ratios for all elements, with the only exception of Ni which is strongly overabundant with respect to the Sun.

4. The Taurus–Auriga region: SU Aur and HD 283572

The Taurus–Auriga region is one of the most active regions of low-mass star formation. It contains protostars, CTT and WTT stars, brown dwarfs and a number of Herbig-Haro objects with protostellar jets. The region extends over many square degrees; its central area, the Taurus Molecular Cloud (TMC) is the objective of an approved XMM-*Newton* Large Program (P.I. M. Güdel) which will map, in the course of AO3, a significant fraction of the region by means of 19 pointings of 30 ks each. A few pointings on the TMC and the nearby Auriga region were obtained prior to the start of this Large Program as part of the GTO and GO time.

We have obtained two observations of the Taurus–Auriga SFR in AO1 centered, respectively, on the WTT star HD 283572 and on the CTT star SU Aur. While the pointing of HD 283572 was contaminated by high background and thus resulted in poor quality RGS and EPIC spectra (Scelsi et al., 2005), the other pointing was more interesting, although only the MOS detectors were operative at the time of the observation and the RGS spectra came out to be very weak (see below). About 130 sources, mostly PMS stars, have been detected in the MOS exposures of this field which had a nominal duration of 130 ks. The light curve of the central source (SU Aur) is highly variable with frequent flares (see Fig. 8). A 3-T fit of the MOS1 spectrum (shown in Fig. 9) gives components with $T_1 = 0.7$ keV, $EM_1 = 1.0 \times 10^{53}$ cm^{-3}, $T_2 = 1.7$ keV, $EM_2 = 2.1 \times 10^{53}$ cm^{-3}, $T_3 = 4.9$ keV, $EM_3 = 1.5 \times 10^{53}$ cm^{-3}, and Fe abundance 0.7 solar. The X-ray luminosity of the source is $L_X = 7.8 \times 10^{30}$ erg s^{-1} in the 0.3–8 keV band, about three orders of magnitude higher than the average X-ray luminosity of the Sun.

The RGS spectrum of SU Aur obtained simultaneously shows only very weak lines and a strong continuum due to the very hot coronal temperature. Emission is strongly reduced above ~10 Å. This prevents an accurate emission measure reconstruction using the same technique mentioned above for the Hyades stars. As a check for consistency, we have simulated the RGS spectrum expected from the MOS best fit model showing that it is consistent with the observed RGS spectrum (see Fig. 10). The very weak nature of the latter one is entirely due to the high temperature of the source and the high-column density ($N_H \sim 3 \times 10^{21}$ cm^{-2}). This is confirmed by HETGS observations of the same source obtained with *Chandra* (Smith et al., in press). Both *Chandra* and XMM-*Newton* show that the X-ray emission of SU Aur is quite different from that reported for the CTT star TW Hya (Kastner et al., 2002; Stelzer and Schmitt, 2004). While the latter was found to be characterized by low coronal temperature (~3 MK), high-density ($n_e \sim 10^{13}$ cm^{-3}) and strong Ne/Fe overabundance – which were interpreted as indications of accretion rather than coronal activity as the origin of the observed X-ray emission – SU Aur appears to be much hotter and consistent with X-ray emission originating in magnetically confined and highly variable coronal structures. Other recent spectral studies of CTTs and WTTs at high resolution (Kastner et al., 2004; Argiroffi et al., 2004, in press) reveal indeed a quite complex picture with no obvious pattern. Clearly, X-ray observations of more CTT stars are required before one can understand the origin of X-rays in these objects, and the relative role played by accretion and magnetically controlled coronal activity.

With regard to the other source (HD 283572) that we observed in Taurus, Scelsi et al. (2005) were able, in spite of the high-background level of this observation and the relatively short nominal exposure time (50 ks), to derive

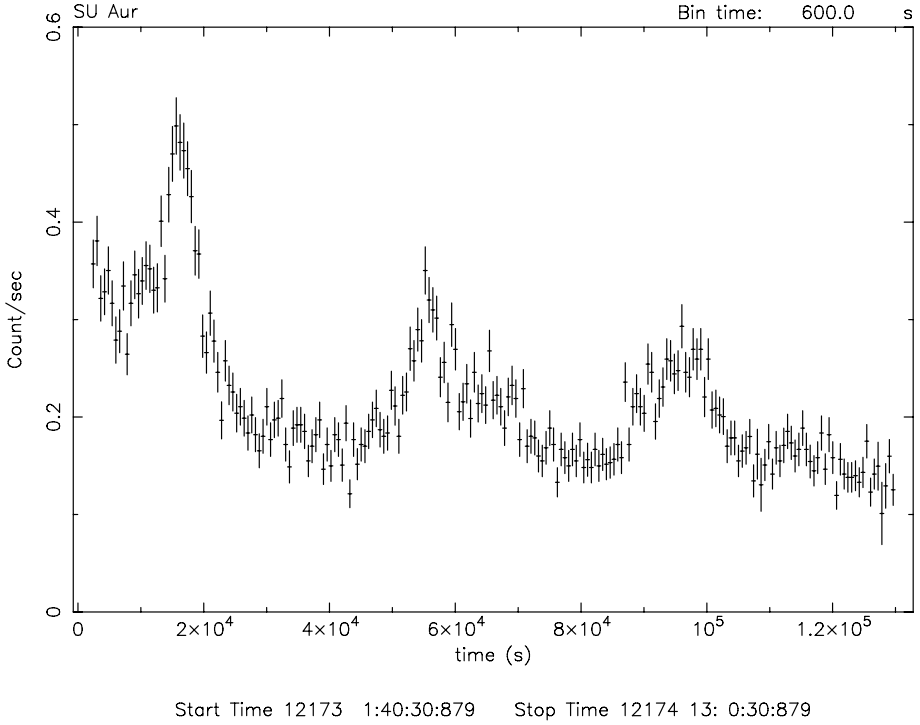

Fig. 8. Frequent flaring in the classical T Tauri star SU Aur as shown by the EPIC MOS light curve.

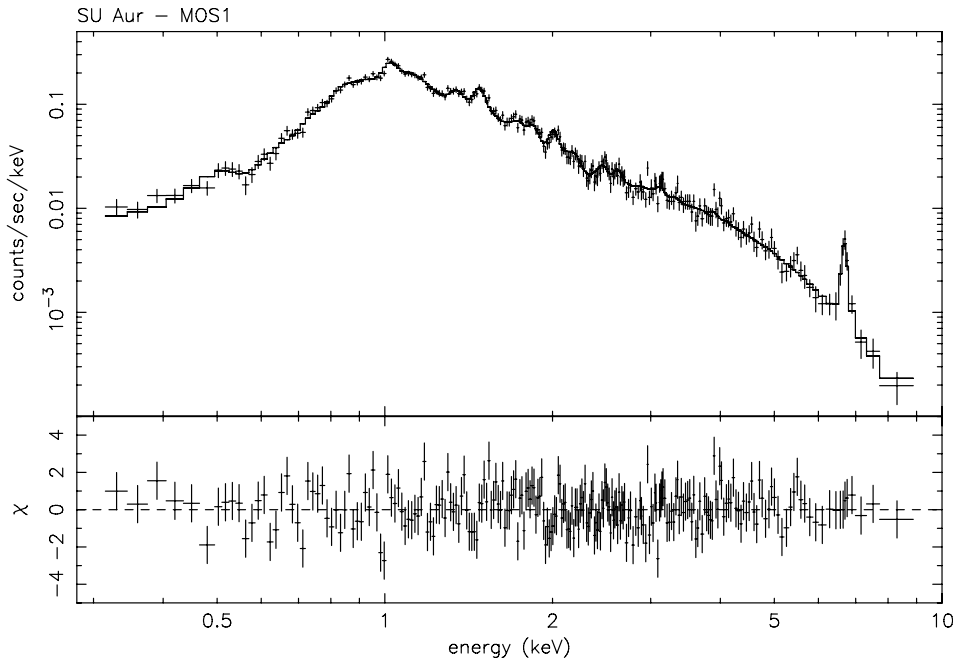

Fig. 9. EPIC MOS1 spectrum of SU Aur (observed and best fit). The residuals are also shown.

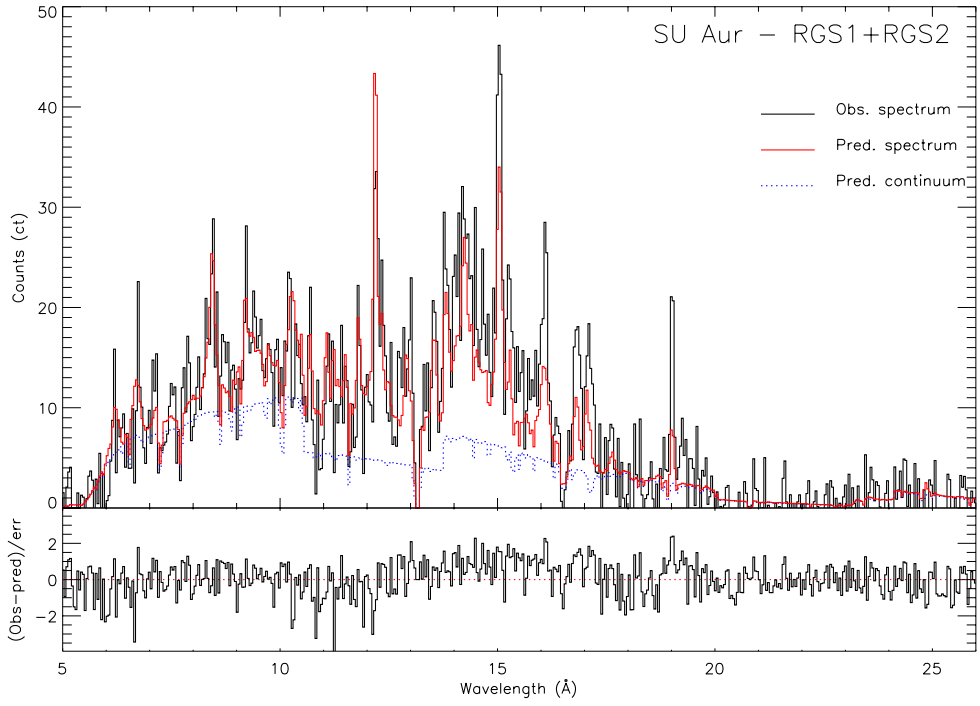

Fig. 10. Comparison of the observed RGS spectrum of SU Aur and of a predicted RGS spectrum computed from EPIC best fit data. The predicted continuum is also shown.

the temperature structure, elemental abundances and $EM(T)$ distribution using both EPIC and RGS data. A 3-T model of the EPIC PN spectrum yields $T_1 = 0.4$ keV, $EM_1 = 3.2 \times 10^{53}$ cm^{-3}, $T_2 = 0.95$ keV, $EM_2 = 3.2 \times 10^{53}$ cm^{-3}, $T_3 = 2.3$ keV, $EM_3 = 5.0 \times 10^{53}$ cm^{-3}, and Fe abundance ~0.4 solar. The hydrogen column density turned out to be $N_H = 8.7 \times 10^{20}$ cm^{-2} and the luminosity in the spectral band 0.3–8 keV to be $L_X = 9.0 \times 10^{30}$ erg s^{-1}. The $EM(T)$ distribution reconstructed from the RGS line spectrum using the MCMC

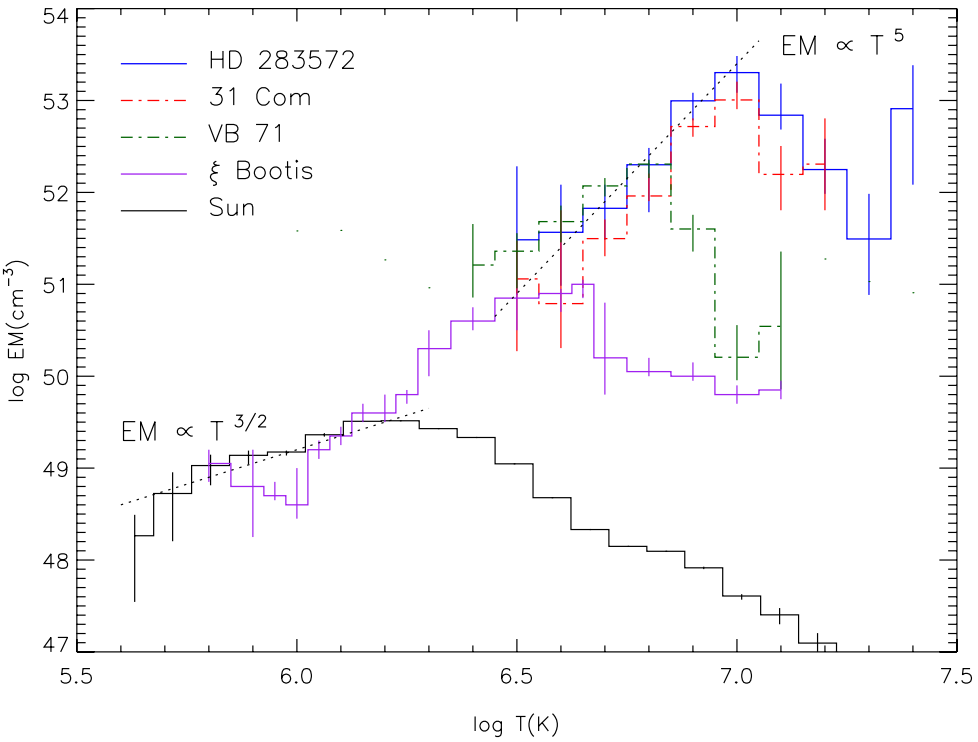

Fig. 11. Emission measure distribution vs. temperature of HD 283572, compared to those of other stars of different activity levels and in different evolutionary states.

method of Kashyap and Drake (1998) is shown in Fig. 11 together with the $EM(T)$ distributions derived in the same way for a number of stars of various activity levels, including the Hyades clump giant VB 71 discussed above and the Sun (the latter one synthesized from spatially resolved *Yohkoh*/SXT data). As shown in the figure, the $EM(T)$ distribution of HD 283572 peaks at $\log T \sim 7.0$ and is very similar to that of the Herzsprung-gap giant 31 Com, in spite of the different evolutionary phases of the two stars. Both stars (which have a similar X-ray luminosity) are significantly hotter and brighter than the Hyades clump giant VB 71, and much hotter than the intermediate-activity MS star ξ Boo and of low-activity stars like the Sun. All active stars show a quite steep power-law rise of the $EM(T)$ from $\log T \sim 6.5$ to the peak (but see Audard et al., 2004 for the different behavior of the extremely active FK Comae-type star YY Men). This slope is much steeper than the one found for the Sun and other inactive stars (which have $EM(T) \sim T^{3/2}$, consistent with uniform heating in constant-pressure, constant-cross-section loops). As discussed by Argiroffi et al. (2003) and Scelsi et al. (2004), this may indicate either heating at the footpoints of coronal loops or loops which expand strongly toward the apex. Note that the reconstructed $EM(T)$ refers in the stellar case to coronal properties *averaged* over the full ensemble of the unresolved loop structures that make up the corona of the star.

The abundance analysis carried out by Scelsi et al. (2005) from the RGS line spectrum of HD 283572 shows subsolar abundances and a pattern of element-to-Fe ratios vs. FIP similar to that observed in 31 Com but different from the one observed in the clump giant VB 71. The abundance ratios of HD 283572 and 31 Com vs. FIP show an initial decrease (with respect to solar photospheric values) down to a shallow minimum around carbon, followed by slightly increasing abundances for elements with higher FIP (see Audard, 2003 for a discussion of the FIP effect in stellar coronae). Overall, the temperature structure and elemental abundances derived for HD 283572 from XMM-*Newton* data are consistent with those derived by Audard et al. (in press) from a *Chandra* HETGS observation of the same star.

5. Conclusions

It is clear from the examples given above that XMM-*Newton* observations of OCs and SFRs are providing important information on the temperature structure, emission measure distribution and elemental abundances of stars of different ages and in different evolutionary states. This information is crucial for understanding magnetic dynamo activity in MS late-type stars and the relative role of accretion vs. magnetic

processes in PMS stars. The few cases presented above allow us to draw the following preliminary conclusions:

(1) Hot stars (exemplified here by σ Ori AB) have softer spectra than cool stars and no convincing evidence of flare-like variability (but see discussion above for the controversial case of the hot magnetically peculiar star σ Ori E). The softer spectra and the absence of flare-like variability argue against solar-like coronal activity and are consistent instead with X-ray emission originating in shocked winds.
(2) All late-type stars are consistent with coronal magnetic activity and usually show significantly lower coronal metal abundances than solar photospheric abundances with some (not yet fully understood) dependence on FIP.
(3) The abundances of C, O, and N in the clump giant VB 71 in the Hyades are consistent with dredge-up of CNO-cycle processed material, as observed in other evolved stars (Ness, 2005).
(4) The emission measure distribution of late-type stars does not seem to depend on the evolutionary stage of the star, as shown by the comparisons of the Hyades stars VB 50 and VB 71 in this paper or of HD 283572 and 31 Com in Scelsi et al. (2005). The $EM(T)$ appears to depend instead on the activity level of the star as measured by its X-ray luminosity.
(5) There is a pattern of increasing maximum coronal temperature and $EM(T)$ vs. T steepness going from inactive stars like the Sun to very active stars like HD 283572 or 31 Com, as previously found by Scelsi et al. (2004).
(6) The comparison of the CTT star SU Aur with the WTT star HD 283572 does not show evidence of any significant difference in their overall coronal properties as could result from a predominant role of accretion in CTT stars. This is confirmed by *Chandra* observations of the same star but is at variance with what reported for the CTT star TW Hya observed by *Chandra* and XMM-*Newton* (Kastner et al., 2002; Stelzer and Schmitt, 2004). No significant difference in the temperature and metallicity of CTT and WTT stars was found by us for a small sample of PMS stars in the σ Ori cluster.

The conclusions above will be tested with further spectroscopic observations of stars in OCs and SFRs to be obtained with XMM-*Newton* and *Chandra*.

Acknowledgments

Based on observations obtained with XMM-*Newton*, an ESA science mission with instruments and contributions directly funded by ESA Member Stars and NASA. The authors acknowledge the financial support of the Italian Space Agency (ASI) and of the Ministry for Education, University and Research (MIUR).

References

Argiroffi, C., Maggio, A., Peres, G. On coronal structures and their variability in active stars: the case of Capella observed with Chandra/LETGS. A&A 404, 1033–1049, 2003.
Argiroffi, C., Drake, J.J., Maggio, A., Peres, G., Sciortino, S., Harnden, F.R. High-resolution X-ray spectroscopy of the Post-T Tauri star PZ Telescopii. ApJ 609, 925–934, 2004.
Argiroffi, C., Maggio, A., Peres, G., Stelzer, B., Neuhäuser, R. XMM-Newton observation of the metal depleted T Tauri star TWA 5, A&A (in press).
Audard, M. Investigations of stellar coronae with XMM-Newton. Adv. Space Res. 32, 927–936, 2003.
Audard, M., Telleschi, A., Güdel, M., Skinner, S.L., Pallavicini, R., Mitra-Kraev, U. Some like it hot: the X-ray emission of the giant star YY Mensae. ApJ 617, 531–550, 2004.
Audard, M., Skinner, S.L., Smith, K.W., Güdel, M., Pallavicini, R. High-energy processes in young stars: Chandra X-ray spectroscopy of HDE 283572, RY Tau, and LkCa 21, in: Favata, F., Schmitt, J.H.M.M. (Eds.), ESA Spec. Publ. (in press).
Béjar, V.J.S., Zapatero-Osorio, M.R., Rebolo, R. A search for very low mass stars and brown dwarfs in the young σ Orionis cluster. ApJ 521, 671–681, 1999.
Béjar, V.J.S., Zapatero-Osorio, M.R., Rebolo, R. Optical and infrared photometry of new very low-mass stars and brown dwarfs in the σ Orionis cluster. AN 325, 705–713, 2004.
Favata, F., Giardino, G., Micela, G., Sciortino, S., Damiani, E. An XMM-Newton-based X-ray survey of pre-main sequence stellar emission in the L1551 star-forming complex. A&A 403, 187–203, 2003.
Feigelson, E.D., Montmerle, T. High-energy processes in Young Stellar Objects. ARA&A 37, 363–408, 1999.
Franciosini, E., Randich, S., Pallavicini, R. XMM-Newton observations of open clusters. Adv. Space Res. 32, 1143–1148, 2003.
Franciosini, E., Pallavicini, R., Sanz-Forcada, J. The σ Orionis open cluster observed with XMM-Newton: source detection and spectral properties, in: Favata, F., Schmitt, J.H.M.M. (Eds.), ESA Spec. Publ. (in press).
Groote, D., Schmitt, J.H.M.M. Discovery of X-ray flaring on the magnetic Bp-star σ Ori E. A&A 418, 235–242, 2004.
Kashyap, V., Drake, J.J. Markov-Chain Monte Carlo reconstruction of emission measure distributions: application to solar extreme-ultraviolet spectra. ApJ 503, 450–466, 1998.
Kastner, J.H., Huenemoerder, D.P., Schulz, N.S., Canizares, C.R., Weintraub, D.A. Evidence for accretion: high-resolution X-ray spectroscopy of the Classical T-Tauri star TW Hydrae. ApJ 567, 434–440, 2002.
Kastner, J.H., Huenemoerder, D.P., Schulz, N.S., Canizares, C.R., Li, J., Weintraub, D.A. The coronal X-ray spectrum of the multiple weak-lined T Tauri star system HD98800. ApJ 605, L49–L52, 2004.
Kenyon, M.J., Jeffries, R.D., Naylor, T., Oliveira, J.M., Maxted, P.F.L. Membership, binarity and accretion among very low-mass stars and brown dwarfs of the σ Orionis cluster. MNRAS 356, 89–106, 2005.
Jeffries, R.D. X-rays from open clusters, in: Butler, C.J., Doyle, J.G. (Eds.), Solar and Stellar Activity: Similarities and Differences, ASP Conf. Ser. 158, pp. 75–86, 1999.

Lambert, D.L., Ries, L.M. Carbon, nitrogen, and oxygen abundances in G and K giants. ApJ 248, 228–248, 1981.

Maggio, A. The coronae of bright late-type stars observed with EPIC and RGS. Mem. S.A.It. 75, 444–447, 2004.

Ness, J.-U. X-ray emission through the stages of stellar activity, Adv. Space Res., 2005 (this volume).

Pallavicini, R., Franciosini, E., Randich, S. XMM-Newton EPIC observations of stellar clusters and star forming regions. Mem. S.A.It. 75, 434–439, 2004.

Randich, S. Coronal activity among open cluster stars, in: Pallavicini, R., Micela, G., Sciortino, S. (Eds.) Stellar Clusters and Associations: Convection, Rotation, and Dynamos, ASP Conf. Ser. 198, pp. 401–410, 2000.

Sanz-Forcada, J., Franciosini, E., Pallavicini, R. XMM-Newton observations of the σ Ori cluster. I. The complex RGS spectrum of the hot star σ Ori AB. A&A 421, 715–727, 2004.

Scelsi, L., Maggio, A., Peres, G., Gondoin, Ph. X-ray spectroscopy of the Herzsprung-gap giant star 31 Com observed with XMM-Newton. A&A 413, 643–655, 2004.

Scelsi, L., Maggio, A., Peres, G., Pallavicini, R. Coronal properties of G-type stars in different evolutionary phases. A&A 432, 671–685, 2005.

Scholz, A., Eislöffel, J. Rotation and accretion of very low mass objects in the σ Ori cluster. A&A 419, 249–267, 2004.

Sherry, W.H., Walter, F.M., Wolk, S.J. Photometric identification of the low-mass population of Orion OBIb. I. The σ Orionis cluster. AJ 128, 2316–2330, 2004.

Smith, K., Audard, M., Güdel. M., Skinner, S., Pallavicini, R. Spot the differences: the X-ray spectrum of SU Aur compared to TW Hya, in: Favata, F., Schmitt, J.H.M.M. (Eds.), ESA Spec. Publ. (in press).

Stassun, K.G., Ardila, D.R., Barsony, M., Basri, G., Mathieu, R.D. X-ray properties of pre-main sequence stars in the Orion Nebula Cluster with known rotation periods. AJ 127, 3537–3552, 2004.

Stelzer, B., Schmitt, J.H.M.M. X-ray emission from a metal depleted accretion shock onto the classical T Tauri star TW Hya. A&A 418, 687–697, 2004.

Stern, R.A., Schmitt, J.H.M.M., Kahabka, P.T. ROSAT All-Sky Survey observations of the Hyades cluster. ApJ 448, 683–704, 1995.

Walter, F.M., Wolk, M., Freyberg, M., Schmitt, J.H.M.M. Discovery of the σ Orionis cluster. Mem. S.A.It. 68, 1081–1088, 1997.

Zapatero-Osorio, M.R., Béjar, V.J.S., Martín, E.L., et al. Discovery of young, isolated planetary mass objects in the σ Orionis star cluster. Science 290, 103–107, 2000.